

Dirac and Weyl Semimetal in $XY\text{Bi}$ ($X=\text{Ba, Eu}$; $Y=\text{Cu, Ag}$ and Au)

Yongping Du¹, Bo Wan¹, Di Wang¹, Li Sheng^{1,2}, Chun-Gang Duan³ and Xiangang Wan^{1,2*}

¹National Laboratory of Solid State Microstructures and Department of Physics, Nanjing University, Nanjing 210093, China

²Collaborative Innovation Center of Advanced Microstructures, Nanjing University, Nanjing 210093, China

³Key Laboratory of Polar Materials and Devices, Ministry of Education, East China Normal University, Shanghai 200062, China

(Dated: October 12, 2018)

Weyl and Dirac semimetals recently stimulate intense research activities due to their novel properties. Combining first-principles calculations and effective model analysis, we predict that nonmagnetic compounds BaYBi ($Y=\text{Au, Ag}$ and Cu) are Dirac semimetals. As for the magnetic compound EuYBi , although the time reversal symmetry is broken, their long-range magnetic ordering cannot split the Dirac point into pairs of Weyl points. However, we propose that partially substitute Eu ions by Ba ions will realize the Weyl semimetal.

PACS numbers: 71.20.-b, 73.20.-r, 71.20.Lp

Following the discovery of topological insulator (TI) [1, 2], there has been considerable research interest in studying the Weyl semimetal (WSM), the first metallic topologically nontrivial matter [3–6]. In WSM, non-degenerate valence and conduction bands touch at an accidental degeneracy point in a three-dimensional (3D) Brillouin zone, and its low energy physics is approximated by the Weyl equation [3, 4]. Weyl points, the nondegenerate linear touchings of the bulk bands, always come in pair, and they are robust due to the protection by the topology of the band structure. The most remarkable feature of WSM is the Fermi arc surface states [3]. Several compounds, including pyrochlore iridates [3], TI based heterostructures [7], HgCr_2Se_4 [8] and many other systems [9–12] had been theoretically predicted as promising WSMs. While the indication about realization of WSM have been reported [13–15], the presence of the Fermi arc, as the smoking-gun feature, unfortunately still has not been confirmed.

Same as the WSM, the Dirac semimetal (DSM) is also a 3D analog of graphene [16–19]. But in contrast with Weyl point, the Dirac point has four-fold degeneracy, and does not possess the a topological number, consequently the Dirac point is not robust to against the external perturbations and usually hard to be realized. Thus the 3D DSM receive much less attention until the discovery of Na_3Bi [20] and Cd_3As_2 [21]. Wang *et al.* find that there is a paired 3D bulk Dirac points exist on the k_z axis of Na_3Bi [20] and Cd_3As_2 [21], and these Dirac points are protected by the crystal symmetry thus are stable [20, 21]. The theoretical propose about Na_3Bi and Cd_3As_2 [20, 21] had been quickly confirmed by the subsequent photoemission measurement [22–25]. This immediately triggers a new wave of research to explore the unique properties associated with the 3D Dirac points in the DSM [22–28]. Unfortunately, Na_3Bi is not stable in air while arsenic limits the application of Cd_3As_2 . Therefore searching new 3D DSM with less toxic and stability in nature is of both fundamental and technological

importance.

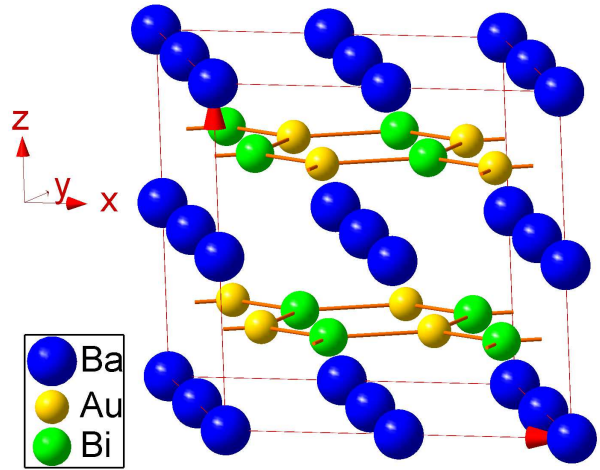


FIG. 1: Crystal structure of BaAuBi . BaAgBi and BaCuBi have similar structure.

In this paper, based on the density functional theory (DFT) calculations and effective low energy models, we predict that BaYBi ($Y=\text{Au, Ag}$ and Cu) are promising 3D Dirac materials. For BaAuBi , the nontrivial topology is due to the band inversion of the Bi- p bonding and antibonding states, while for the BaAgBi and BaCuBi , the band inversion happens between the Ag/Cu s and Bi p orbital. Protected by the C_3 rotation symmetry, the Dirac points locate along the $\Gamma - A$ line. The magnetic configuration in EuYBi indeed break the time reversal symmetry, however cannot split the Dirac point into two Weyl points. We propose that partially substituting Eu by Ba, i.e. alloy compound $\text{Ba}_x\text{Eu}_{(1-x)}\text{Ag}(\text{Au})\text{Bi}$, which could be grown using molecular beam epitaxy (MBE) technique, is a promising way to realize the WSM.

The electronic band structure calculations have been carried out using the full potential linearized augmented

plane wave method as implemented in WIEN2K package [29]. The modified Becke-Johnson exchange potential together with local-density approximation for the correlation potential (MBJLDA) has been used here to obtain accurate band inversion strength and band order [30]. A $16 \times 16 \times 7$ mesh is used for the Brillouin zone integral. Using the second-order variational procedure, we include the spin-orbital coupling (SOC) interaction.

BaYBi ($Y=\text{Au,Ag,Cu}$) crystallize in the same hexagonal ZrBeSi type structure with space group $P6_3/mmc$ (D_{6h}^4) [31]. The crystal structure of BaAuBi is shown as an example in Fig.1, in which Au and Bi ions form honeycomb lattice layers stacking along c axis and sandwiched by trigonal layers formed by Ba atoms. There are two formula units in the primitive unit cell, and the six atoms in the unit cell can be classified as three nonequivalent crystallographic sites: Ba, Au and Bi according to the symmetry. Ba locate at the $2a$ ($0, 0, \frac{1}{2}$), while Ag and Bi occupy the $2c$ ($\frac{1}{3}, \frac{2}{3}, \frac{1}{4}$) and $2d$ ($\frac{2}{3}, \frac{1}{3}, \frac{1}{4}$) sites, there is no free internal coordinates, and the lattice constants are the only structural parameter for BaYBi lattice. We optimize the lattice parameter and for all of the three compounds, our numerical lattice constants are in good agreements with experiments, and the small discrepancy between the numerical and experimental structure has negligible effect on the electronic structure. Hence, the following results are obtained based on the experimental structure, unless stated specifically.

We first calculate the electronic structure of BaAuBi, and show the results in Fig.2(a). The Ba in BaAuBi is highly ionic, has negligible contribution around Fermi level. Au- $6s$ and $5d$ bands mainly located at -4 to -1 eV, and -6 to -4 eV, respectively. The Bi- $6s$ is basically located about -11 eV below the Fermi level. The valence and conduction bands are dominated by the Bi- $6p$ bonding and antibonding states. Checking the wave function, we find that at the Γ point the Bi- $6p$ antibonding state is higher than the Bi- $6p$ bonding state, however at the A point, the odd-parity state is about 0.545 eV lower in energy than even-parity state.

In order to understand the mechanism of the band inversion, we illustrate the band evolution at the Γ point of BaAuBi at Fig.2(b). As discuss above, the states near Fermi level are primarily contributed by the Bi- $6p$ orbital, with also the Au- $6s$ state. Since the two Bi atoms (Bi and Bi') in the unit cell are related to each other by the inversion symmetry, similar with Ref.[32, 33], we combine the Bi- $6p$ orbitals to form the hybridized states and label the bonding and antibonding states as $|P_{x,y,z}^+\rangle$ ($|P_{x,y,z}^+\rangle = \frac{1}{\sqrt{2}}(|\text{Bi}, p_{x,y,z}\rangle - |\text{Bi}', p_{x,y,z}\rangle)$) and $|P_{x,y,z}^-\rangle$ ($|P_{x,y,z}^-\rangle = \frac{1}{\sqrt{2}}(|\text{Bi}, p_{x,y,z}\rangle + |\text{Bi}', p_{x,y,z}\rangle)$) respectively, where the superscripts $+/-$ denote the parity of the corresponding states. According to the point group symmetry, the p_z orbital split from the p_x and p_y orbitals while the latter two still degenerate as shown in the Fig.2(b).

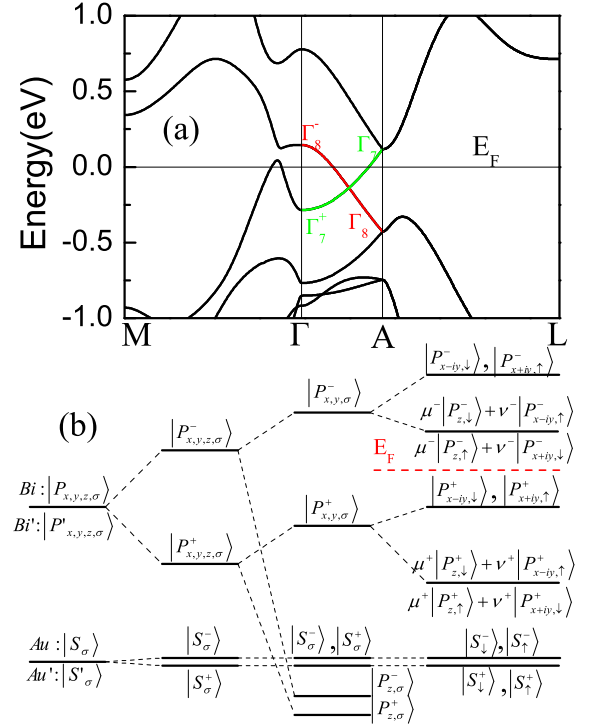


FIG. 2: (a) Electronic structure of BaAuBi. Green and red line highlights the different irreducible representation along $\Gamma - A$. (b) Band evolution near Fermi energy of BaAuBi at Γ point, red dashed line stands for the Fermi energy (see main text for detailed description).

Finally, we consider the effect of SOC. The $|P_{x+iy,\uparrow}^+\rangle$ and $|P_{x-iy,\downarrow}^+\rangle$ states are pushed up by the SOC, while the $|P_{z,\uparrow}^-\rangle$ ($|P_{z,\downarrow}^-\rangle$) will mix with $|P_{x+iy,\downarrow}^-\rangle$ ($|P_{x-iy,\uparrow}^-\rangle$), consequently the bonding ($|P_{x+iy,\uparrow}^+\rangle$ and $|P_{x-iy,\downarrow}^+\rangle$) and antibonding states ($\mu^-|P_{z,\uparrow}^-\rangle + \nu^-|P_{x+iy,\downarrow}^-\rangle$ and $\mu^-|P_{z,\downarrow}^-\rangle + \nu^-|P_{x-iy,\uparrow}^-\rangle$) are close to each other at the Γ point, and the band inversion occurs at the A point as shown in Fig.2.

Along $\Gamma - A$ line the C_3 symmetry is reserved, by the symmetry analysis the two relevant bands along this line belong to different representations (Γ_7 and Γ_8 as shown in Fig.2(a). See the appendix for the detail). Thus the hybridization between these bands is strictly forbidden, which results in the protected band crossing as shown in Fig.2(a). The Dirac point is located slightly below the Fermi level as shown in Fig.2(a), and the novel properties associated with DSM can be observed in BaAuBi.

Since the topological nature is determined by the Γ_7 and Γ_8 bands, based on the projection-operator method (see the appendix), we build the effective Hamiltonian by using the four relevant states as bases (in the order of $|P_{x+iy,\uparrow}^+\rangle$, $\mu^-|P_{z,\downarrow}^-\rangle + \nu^-|P_{x-iy,\uparrow}^-\rangle$, $|P_{x-iy,\downarrow}^+\rangle$, $\mu^-|P_{z,\uparrow}^-\rangle + \nu^-|P_{x+iy,\downarrow}^-\rangle$) at Γ point. We neglect all of other states, since they are far from the Fermi level and not involve

into the band inversion, and the Hamiltonian can be written as:

$$H_{eff} = \epsilon_0(\mathbf{k}) + \begin{pmatrix} M(\mathbf{k}) & A(\mathbf{k})k_+ & 0 & Bk_zk_+^2 \\ A(\mathbf{k})k_- & -M(\mathbf{k}) & -Bk_zk_+^2 & 0 \\ 0 & -Bk_zk_-^2 & M(\mathbf{k}) & A(\mathbf{k})k_- \\ Bk_zk_-^2 & 0 & A(\mathbf{k})k_+ & -M(\mathbf{k}) \end{pmatrix}$$

where $\epsilon_0(\mathbf{k}) = C_0 + C_1k_z^2 + C_2(k_x^2 + k_y^2)$, $M(\mathbf{k}) = M_0 - M_1k_z^2 - M_2(k_x^2 + k_y^2)$, $A(\mathbf{k}) = A_0 + A_1k_z^2 + A_2(k_x^2 + k_y^2)$ and $k_{\pm} = k_x \pm ik_y$. The parameters in the above formula are material dependent, and by fitting the DFT calculated band dispersion, we obtain $C_0 = -0.06978\text{eV}$, $C_1 = -0.34038\text{eV} \cdot \text{\AA}^2$, $C_2 = 2.25\text{eV} \cdot \text{\AA}^2$, $M_0 = -0.21537\text{eV}$, $M_1 = -1.9523\text{eV} \cdot \text{\AA}^2$, $M_2 = -7.9507\text{eV} \cdot \text{\AA}^2$, and $A_0 = 1.3668\text{eV} \cdot \text{\AA}$. Solving the above eigenvalue problem, we obtain $E(\mathbf{k}) = \epsilon_0(\mathbf{k}) \pm \sqrt{M(\mathbf{k})^2 + A(\mathbf{k})^2k_+k_- + |B|^2k_z^2k_+^2k_-^2}$, and at $\mathbf{k}_c = (0, 0, \pm\sqrt{\frac{M_0}{M_1}})$, we get the gapless solutions. In the vicinity of \mathbf{k}_c and neglect the high-order terms, $E(\mathbf{k}')$ would be equal to $\epsilon_0(\mathbf{k}') \pm \sqrt{4M_1^2\mathbf{k}_c^2\delta k_z^2 + A^2(\mathbf{k}_c)(\delta k_x^2 + \delta k_y^2)}$ ($\delta k_{x,y,z}$ are small displacement from \mathbf{k}_c), which is a linear dispersion and suggests in neighbourhood of \mathbf{k}_c , our effective Hamiltonian is nothing but 3D anisotropic massless Dirac fermions.

We also investigate the BaAgBi and BaCuBi. The electronic properties of BaCuBi are very similar with that of BaAgBi, we thus only discuss BaAgBi at following. As shown in Fig.3(b), sharply contrast to the Au-6s state in BaAuBi, the Ag-5s orbital in BaAgBi is higher in energy than Bi-6p state, consequently the states closed to the Fermi level become $|P_{x+iy,\uparrow}^- \rangle$, $|P_{x-iy,\downarrow}^- \rangle$ and $|S_{\uparrow}^+ \rangle$, $|S_{\downarrow}^+ \rangle$. Similar with the case in Na₃Bi[20], due to the strong SOC of Bi-6p, the $|P_{x+iy,\uparrow}^- \rangle$ and $|P_{x-iy,\downarrow}^- \rangle$ states will be pushed up, which results in the band inversion at Γ point. This inversion is confirmed by our DFT calculation, as shown in Fig.3(a), at the Γ point, the $|P_{x+iy,\uparrow}^- \rangle$, $|P_{x-iy,\downarrow}^- \rangle$ is higher than $|S_{\uparrow}^+ \rangle$, $|S_{\downarrow}^+ \rangle$ by about 0.34 eV. Along $\Gamma - A$ line, these two bands belongs to different (Γ_7 and Γ_8) representations, thus there is also an unavoidable crossing point located at $\Gamma - A$ line. It is also easy to prove that around the band touching points, the band dispersion is linear, thus the crossing points are the Dirac points.

It is well known that breaking the time reversal symmetry will split the Dirac point into two Weyl points. This family of intermetallic compound with hexagonal structure indeed has several members with magnetic ion Eu: EuXY ($X=\text{Cu, Au, Ag}$; $Y=\text{As, Sb, Bi}$) [31, 34, 35]. Experiments confirm that some of them indeed possess long-range magnetic configuration [34]. Unfortunately, the Eu²⁺ spins align ferromagnetically with the ab plane, but antiferromagnetically along the c -axis[35], therefore the exchange field is exactly cancelled at the XY -plane of EuXY. Thus breaking the time reversal symmetry by

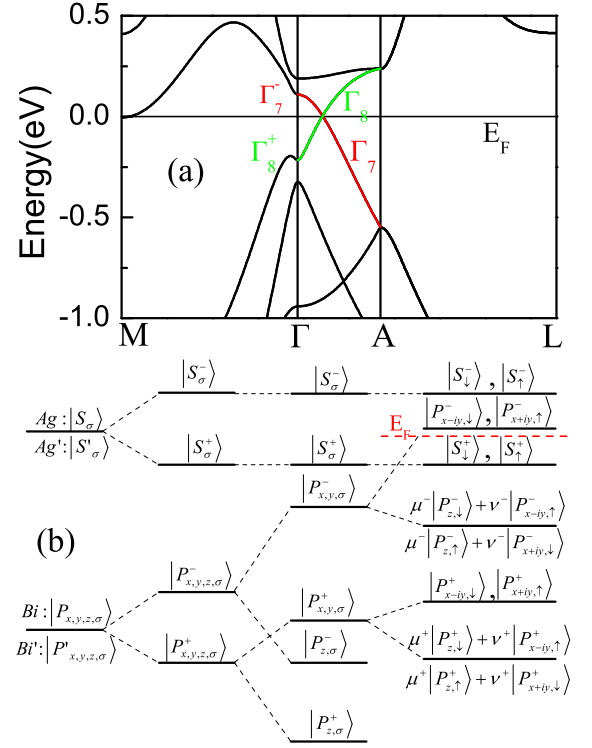


FIG. 3: (a) Electronic structure of BaAgBi, Green and red line highlights the different irreducible representation along $\Gamma - A$. (b) Band evolution around Fermi energy of BaAgBi at Γ point, red dashed line stands for the Fermi energy.

this type of antiferromagnetic configuration cannot split the Dirac points, and the compounds of EuXY have no chance to become WSM.

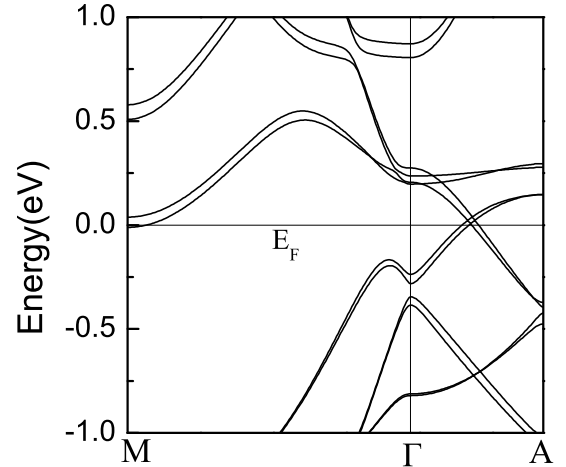


FIG. 4: Calculated band structure of Eu_{0.5}Ba_{0.5}AgBi

We, however, expect that substituting part of Eu ions by Ba ions, the two antiferromagnetically coupled Eu

plane in $\text{Eu}_x\text{Ba}_{1-x}\text{AgBi}$ may not exactly cancel each other, and then there is a chance the compound becomes WSM. To confirm this expectation, we then performed another calculation on $\text{Eu}_{0.5}\text{Ba}_{0.5}\text{AgBi}$, in which we replace one of the two antiferromagnetically coupled Eu plane in the unit cell by Ba. As shown in Fig.4, the Dirac point indeed splits into two Weyl points, and $\text{Eu}_{0.5}\text{Ba}_{0.5}\text{AgBi}$ becomes WSM. We argue that such structure can be typically synthesized using the cutting-edge film growth technique like MBE. Therefore we believe that WSM can be realized in the above discussed structures.

In summary, based on density-functional calculation and effective model analysis, we propose that the BaYBi ($Y=\text{Au}$, Ag and Cu) are 3D Dirac semimetals. The nontrivial topological feature is due to p - p inversion for BaAuBi and s - p band inversion for BaAgBi and BaCuBi , and their Dirac points are protected by the C_3 rotation symmetry. Their magnetic cousins, i.e EuYBi ($Y=\text{Au}$, Ag and Cu) are not Weyl semimetals. However, partial substitution of Eu with Ba ions in EuYBi could result in the Weyl semimetal. Furthermore, our numerical calculation also confirm that a uniaxial strain along a -axis, which breaks the C_3 rotation symmetry, will drive BaAgBi into topological insulator.

Note. When finalizing our work, we became aware of a recent study by Borisenko *et al.* [36], in which the authors also predict BaAgBi is a possible 3D DSM, agreeing with our conclusion.

The work was supported by the National Key Project for Basic Research of China (Grants No. 2011CB922101, 2014CB921104), NSFC under Grants No. 91122035, 11174124, 11374147 and 61125403. The project is also funded by Priority Academic Program Development of Jiangsu Higher Education Institutions.

APPENDIX

Effective Hamiltonian for BaAuBi

The conduction and valence bands of BaAuBi are mainly contributed by four states: $\left|P_{x+iy,\uparrow}^+\right\rangle$, $\mu^- \left|P_{z,\downarrow}^-\right\rangle + \nu^- \left|P_{x-iy,\uparrow}^-\right\rangle$, $\left|P_{x-iy,\downarrow}^+\right\rangle$ and $\mu^- \left|P_{z,\uparrow}^-\right\rangle + \nu^- \left|P_{x+iy,\downarrow}^-\right\rangle$, we thus use these states as the basis to build the effective model Hamiltonian at the Γ point of BZ. As a 4×4 hermitian matrix, the effective Hamiltonian can be written as $H = \epsilon(\mathbf{k})\mathbf{I} + \sum_i d_i(\mathbf{k})\Gamma_i + \sum_{ij} d_{ij}(\mathbf{k})\Gamma_{ij}$, where \mathbf{I} is the 4×4 identity matrix, Γ_i and Γ_{ij} are Dirac matrices, $\epsilon(\mathbf{k})$, $d_i(\mathbf{k})$, and $d_{ij}(\mathbf{k})$ are function of momentum k .

The Hamiltonian should be invariant under the operation of crystal symmetry and time reversal symmetry. This requires the function $d_i(\mathbf{k})$ [$d_{ij}(\mathbf{k})$] and the associated Γ_i [Γ_{ij}] matrices belong to the same irreducible representation.

Thus the key problem is to determine the irreducible representation for $d_i(\mathbf{k})$ [$d_{ij}(\mathbf{k})$] and Γ matrices, which can be done by the projection-operator method.

The Dirac Γ matrices can be written as $\Gamma_1 = \sigma_1 \otimes \tau_1$, $\Gamma_2 = \sigma_2 \otimes \tau_1$, $\Gamma_3 = \sigma_3 \otimes \tau_1$, $\Gamma_4 = \sigma_0 \otimes \tau_2$, $\Gamma_5 = \sigma_0 \otimes \tau_3$, and $\Gamma_{ab} = [\Gamma_a, \Gamma_b]/2i$ [33]. The projection operator is defined as $p^i = \frac{l_i}{g} \sum_{R \in G} \chi^i(R)P_R$, where g is the group

order, l_i is the dimension of the i th representation, R denotes the group element i.e. the symmetry operation, $\chi^i(R)$ represent the character of group element R in i th representation, P_R is the operator of group element R .

The double group of D_{6h}^4 has 18 classes, and their irreducible representations are denoted as R_1 to R_{18} [37], and its character table can be found in Ref[37]. Based on the basis mentioned above, one can easily work out the transformation matrix D_R for symmetry operator P_R , which allow us to apply the projection operator p^i on Γ_a : $p^i \Gamma_a = \frac{l_i}{g} \sum_{R \in G} \chi^i(R)D_R \Gamma_a D_R^{-1}$, consequently determine the irreducible representation of Γ_a .

Using the same process, one can also determine the irreducible representation for the polynomials of \mathbf{k} up to $O(\mathbf{k}^3)$. We present the irreducible representation of Dirac Γ matrices and polynomials of \mathbf{k} , and their transformation under time reversal in Table I.

With the Table I, the effective model Hamiltonian of BaAuBi can be easily expressed as: $H = \epsilon_0(\mathbf{k}) + M(\mathbf{k})\Gamma_5 + A(\mathbf{k})(k_x\Gamma_{45} + k_y\Gamma_{35}) + Bk_z((k_x^2 - k_y^2)\Gamma_{25} + 2k_xk_y\Gamma_{15})$, where $\epsilon_0(\mathbf{k}) = C_0 + C_1k_z^2 + C_2(k_x^2 + k_y^2)$, $M(\mathbf{k}) = M_0 - M_1k_z^2 - M_2(k_x^2 + k_y^2)$, $A(\mathbf{k}) = A_0 + A_1k_z^2 + A_2(k_x^2 + k_y^2)$.

Effective Hamiltonian for BaAgBi

For BaAgBi , the conduction bands are Ag-5s states, while the valence bands are Bi-6p states, thus the four basis become $\left|S_{\uparrow}^+\right\rangle$, $\left|P_{x+iy,\uparrow}^-\right\rangle$, $\left|S_{\downarrow}^+\right\rangle$ and $\left|P_{x-iy,\downarrow}^-\right\rangle$. We list the character table of Γ matrices and the function $d(\mathbf{k})$ (expanded as polynomials of the momentum k) and their transformation under time reversal in Table II. Based on Table II, one can get the effective model Hamiltonian for BaAgBi : $H = \epsilon_0(\mathbf{k}) + M(\mathbf{k})\Gamma_5 + A(\mathbf{k})(k_x\Gamma_3 - k_y\Gamma_4) + Bk_z((k_x^2 - k_y^2)\Gamma_1 + 2k_xk_y\Gamma_2)$, where $\epsilon_0(\mathbf{k}) = C_0 + C_1k_z^2 + C_2(k_x^2 + k_y^2)$, $M(\mathbf{k}) = M_0 - M_1k_z^2 - M_2(k_x^2 + k_y^2)$, $A(\mathbf{k}) = A_0 + A_1k_z^2 + A_2(k_x^2 + k_y^2)$.

Band representation

At the Γ point of BZ, each state should belong to an irreducible representation of the double group of D_{6h}^4 . Again, applying the projection operator onto the conduction and valence states of BaAuBi , we find that $\left|P_{x+iy,\uparrow}^+\right\rangle$ and $\left|P_{x-iy,\downarrow}^+\right\rangle$ belong to representation

Γ matrices	representation	T
Γ_0, Γ_5	R_1	+
$\{\Gamma_1, \Gamma_2\}$	R_{14}	+
$\{\Gamma_3, \Gamma_4\}$	R_{15}	+
Γ_{12}, Γ_{34}	R_2	-
$\Gamma_{14} + \Gamma_{23}$	R_3	-
$\Gamma_{13} - \Gamma_{24}$	R_4	-
$\{\Gamma_{13} + \Gamma_{24}, \Gamma_{14} - \Gamma_{23}\}$	R_6	-
$\{\Gamma_{15}, \Gamma_{25}\}$	R_{14}	-
$\{\Gamma_{35}, \Gamma_{45}\}$	R_{15}	-
$d(k)$	representation	T
$C, k_z^2, k_x^2 + k_y^2$	R_1	+
$\{k_x k_y k_z, \frac{1}{2}(k_x^2 - k_y^2)k_z\}$	R_{14}	-
$\{k_x, k_y\}, \{(k_x^2 + k_y^2)k_x, (k_x^2 + k_y^2)k_y\}, \{k_z^2 k_x, k_z^2 k_y\}$	R_{15}	-
$k_z, (k_x^2 + k_y^2)k_z, k_z^3$	R_{11}	-
$\{k_x^2 - k_y^2, k_x k_y\}$	R_5	+
$\{k_x k_z, k_y k_z\}$	R_6	+
$k_x^3 - 3k_x k_y^2$	R_{12}	-
$k_y^3 - 3k_x^2 k_y$	R_{13}	-

TABLE I: The character table of Dirac Γ matrices and the polynomials of the momentum k for BaAuBi.

Γ matrices	representation	T
Γ_0, Γ_5	R_1	+
$\{\Gamma_1, \Gamma_2\}$	R_{14}	-
$\{\Gamma_3, \Gamma_4\}$	R_{15}	-
Γ_{12}, Γ_{34}	R_2	-
$\Gamma_{14} - \Gamma_{23}$	R_3	-
$\Gamma_{13} + \Gamma_{24}$	R_4	-
$\{\Gamma_{13} - \Gamma_{24}, \Gamma_{14} + \Gamma_{23}\}$	R_6	-
$\{\Gamma_{15}, \Gamma_{25}\}$	R_{14}	+
$\{\Gamma_{35}, \Gamma_{45}\}$	R_{15}	+
$d(k)$	representation	T
$C, k_z^2, k_x^2 + k_y^2$	R_1	+
$\{k_x k_y k_z, \frac{1}{2}(k_x^2 - k_y^2)k_z\}$	R_{14}	-
$\{k_x, k_y\}, \{(k_x^2 + k_y^2)k_x, (k_x^2 + k_y^2)k_y\}, \{k_z^2 k_x, k_z^2 k_y\}$	R_{15}	-
$k_z, (k_x^2 + k_y^2)k_z, k_z^3$	R_{11}	-
$\{k_x^2 - k_y^2, k_x k_y\}$	R_5	+
$\{k_x k_z, k_y k_z\}$	R_6	+
$k_x^3 - 3k_x k_y^2$	R_{12}	-
$k_y^3 - 3k_x^2 k_y$	R_{13}	-

TABLE II: The character table of Dirac matrices and the function $d(k)$ of BaAgBi.

D_{6h}^4	Γ_7^+	Γ_8^+	Γ_9^+	Γ_7^-	Γ_8^-	Γ_9^-
C_{6v}^1	Γ_7	Γ_8	Γ_9	Γ_7	Γ_8	Γ_9

TABLE III: The compatibility relations between the double group of C_{6v}^1 and D_{6h}^4 .

Γ_7^+ , while $\mu^- \left| P_{z,\downarrow}^- \right\rangle + \nu^- \left| P_{x-iy,\uparrow}^- \right\rangle$ and $\mu^- \left| P_{z,\uparrow}^- \right\rangle +$

$\nu^- \left| P_{x+iy,\downarrow}^- \right\rangle$ belong to representation Γ_8^- , which had been marked in Fig.2(a). Different from Γ point, the symmetry of $\Gamma - A$ line is C_{6v}^1 . We show the compatibility relations between the double group of D_{6h}^4 and C_{6v}^1 in Table III. It is clear that the representation Γ_7^+ and Γ_8^- , evolve to Γ_7 and Γ_8 , respectively.

For BaAgBi, the valence/conduction states at the Γ point of BZ belong Γ_8^+/Γ_7^- , and will change to Γ_8 and Γ_7

along $\Gamma - A$ line according to Table III.

* Corresponding author: xgwan@nju.edu.cn

- [1] M. Z. Hasan and C. L. Kane, *Rev. Mod. Phys.* **82**, 3045 (2010).
- [2] X.L. Qi and S.-C. Zhang, *Rev. Mod. Phys.* **83**, 1057 (2011).
- [3] X. Wan, A. M. Turner, A. Vishwanath, and S. Y. Savrasov, *Phys. Rev. B* **83**, 205101 (2011).
- [4] L. Balents, *Physics* **4**, 36 (2011).
- [5] Y. Ando, *J. Phys. Soc. of Jpn.* **82**, 102001 (2013).
- [6] K.-Y. Yang, Y.-M. Lu, and Y. Ran, *Phys. Rev. B* **84**, 075129 (2011).
- [7] A. A. Burkov and L. Balents, *Phys. Rev. Lett.* **107**, 127205 (2011).
- [8] G. Xu, H. M. Weng, Z. Wang, X. Dai, and Z. Fang, *Phys. Rev. Lett.* **107**, 186806 (2011).
- [9] D. Bulmash, C.-X. Liu, and X.-L. Qi, *Phys. Rev. B* **89**, 081106 (2014).
- [10] G. Halasz and L. Balents, *Phys. Rev. B* **85**, 035103 (2012).
- [11] J. Liu and D. Vanderbilt, *Phys. Rev. B* **90**, 155316 (2014).
- [12] J. L. Manes, *Phys. Rev. B* **85**, 155118 (2012).
- [13] K. Ueda, J. Fujioka, Y. Takahashi, T. Suzuki, S. Ishiwata, Y. Taguchi, and Y. Tokura, *Phys. Rev. Lett.* **109**, 136402 (2012).
- [14] J.-H. Chu, S. C. Riggs, M. Shapiro, J. Liu, C. R. Serero, D. Yi, M. Melissa, S. J. Suresha, C. Frontera, A. Vishwanath, X. Marti, I. R. Fisher, R. Ramesh, arXiv:1309.4750 (2013).
- [15] H.-J. Kim, K.-S. Kim, J.-F. Wang, M. Sasaki, N. Satoh, A. Ohnishi, M. Kitaura, M. Yang, and L. Li, *Phys. Rev. Lett.* **111**, 246603 (2013).
- [16] S. M. Young, S. Zaheer, J. C. Y. Teo, C. L. Kane, E. J. Mele, and A. M. Rappe, *Phys. Rev. Lett.* **108**, 140405 (2012).
- [17] B. Singh, A. Sharma, H. Lin, M. Z. Hasan, R. Prasad, and A. Bansil, *Phys. Rev. B* **86**, 115208 (2012).
- [18] J. A. Steinberg, S. M. Young, S. Zaheer, C. L. Kane, E. J. Mele, and A. M. Rappe, *Phys. Rev. Lett.* **112**, 036403 (2014).
- [19] B. J. Yang and N. Nagaosa, *Nature Communications* **5**, 4898 (2014).
- [20] Z. Wang, Y. Sun, X.-Q. Chen, C. Franchini, G. Xu, H. M. Weng, X. Dai, and Z. Fang, *Phys. Rev. B* **85**, 195320 (2012).
- [21] Z. Wang, H. M. Weng, Q. Wu, X. Dai, and Z. Fang, *Phys. Rev. B* **88**, 125427 (2013).
- [22] Z. K. Liu, B. Zhou, Y. Zhang, Z. J. Wang, H. M. Weng, D. Prabhakaran, S. K. Mo, Z. X. Shen, Z. Fang, X. Dai, Z. Hussain and Y. L. Chen, *Science* **343**, 864 (2014).
- [23] S.-Y. Xu, C. Liu, S. K. Kushwaha, T.-R. Chang, J. W. Krizan, R. Sankar, C. M. Polley, J. Adell, T. Balasubramanian, K. Miyamoto, N. Alidoust, G. Bian, M. Neupane, I. Belopolski, H.-T. Jeng, C.-Y. Huang, W.-F. Tsai, H. Lin, F. C. Chou, T. Okuda, A. Bansil, R. J. Cava, M. Z. Hasan, arXiv:1312.7624 (2013).
- [24] S. Borisenko, Q. Gibson, D. Evtushinsky, V. Zabolotnyy, B. Buechner, R. J. Cava, *Phys. Rev. Lett.* **113**, 027603 (2014).
- [25] M. Neupane, S.-Y. Xu, R. Sankar, N. Alidoust, G. Bian, C. Liu, I. Belopolski, T.-R. Chang, H.-T. Jeng, H. Lin, A. Bansil, F. Chou and M. Z. Hasan, *Nature Communications* **5**, 3786 (2014).
- [26] L. P. He, X. C. Hong, J. K. Dong, J. Pan, Z. Zhang, J. Zhang, S. Y. Li, arXiv:1404.2557 (2014).
- [27] T. Liang, Q. Gibson, M. N. Ali, M. Liu, R. J. Cava, N. P. Ong, arXiv:1404.7794 (2014).
- [28] M. Novak, S. Sasaki, K. Segawa, Y. Ando, arXiv:1408.2183 (2014).
- [29] P. Blaha, K. Schwarz, G. K. H. Madsen, D. Kvasnicka, and J. Luitz, WIEN2K, An Augmented Plane Wave+ Local Orbitals Program for Calculating Crystal Properties (Karlheinz Schwarz, Technische Universitat Wien, Austria, 2001).
- [30] F. Tran and P. Blaha, *Phys. Rev. Lett.* **102**, 226401 (2009).
- [31] F. Merlo, M. Pani and M. L. Fornasini, *J. Less-Common Metals* **166**, 319 (1990).
- [32] H. Zhang, C. X. Liu, X. L. Qi, X. Dai, Z. Fang and S. C. Zhang, *Nature Phys.* **5**, 438 (2009).
- [33] C.-X. Liu, X.-L. Qi, H. Zhang, X. Dai, Z. Fang, and S.-C. Zhang, *Phys. Rev. B* **82**, 045122 (2010).
- [34] G. Michels, S. Junk, W. Schlabitz, E. Holland-Moritz, M. M. Abd-Elmeguid, J. Dunner and A. Mewis, *J. Phys.: Condens. Matter* **6**, 1769 (1994).
- [35] J. Tong, J. Parry, Q. Tao, C.-H. Cao, Z.-A. Xu and H. Zeng, *J. Alloys Compounds* **602**, 26 (2014).
- [36] Q. D. Gibson, L. M. Schoop, L. Muechler, L. S. Xie, M. Hirschberger, N. P. Ong, R. Car, R. J. Cava, arXiv:1411.0005 (2014).
- [37] C. J. Bradley, A. P. Cracknell, *The Mathematical Theory of Symmetry in Solids: Representation Theory for Point Groups and Space Groups*, Oxford University Press, reprinted (2011).